Z. Phys. D 41, 187–193 (1997)

ZEITSCHRIFT
FÜR PHYSIK D

Vicinage effects in the stopping power of H_3^+ beams in amorphous carbon

F. Javier Pérez-Pérez[1], **Cristian D. Denton**[1], **Isabel Abril**[1], **Rafael Garcia-Molina**[2], **Néstor R. Arista**[3]

[1] Departament de Física Aplicada, Universitat d'Alacant, Apartat 99, E-03080 Alacant, Spain
[2] Departamento de Física, Universidad de Murcia, Apartado 4021, E-30080 Murcia, Spain
[3] Instituto Balseiro, Centro Atómico Bariloche, 8400 Bariloche, Argentina

Received: 9 October 1996 / Final version: 2 April 1997

Abstract. The stopping power of H_3^+ molecular beams incident on amorphous carbon foils is analyzed as a function of the orientation of the molecule relative to its direction of motion. The electronic stopping power was calculated within the dielectric formalism, taking into account the dynamics of the Coulomb repulsion among the molecular partners. At intermediate velocities, $v \simeq 2$ a.u., the stopping ratio for the perpendicular orientation is greater than for the parallel one, while the opposite behaviour is shown for higher velocities. The stopping ratio for randomly oriented H_3^+ molecules was evaluated for different target thicknesses, resulting in larger values for the thinner targets and the higher energies. Comparison of our results with available experimental data shows a reasonable agreement.

PACS: 34.50.Bw; 36.40.-c

I Introduction

The study of the interaction of swift ion beams with matter has received a renewed interest in the last years, with recent experiments and theoretical studies using molecular beams as a new tool to prove or modify the structure of matter [1]. The wide area of interest includes basic studies on the interaction of molecular and ion beams with solids and surfaces [2], as well as possible applications to inertial confinement and ion-beam fusion [3].

One of the questions of interest, from the theoretical point of view, is to study the differences that appear when a single charge or an ensemble of charges with a well defined geometrical structure (like a molecular ion) interact with matter. The differences in the energy loss of a fast molecule with respect to the energy loss of its atomic constituents, independently considered, were theoretically predicted and experimentally observed by Brandt et al. [4] in 1974. To quantify these differences the stopping ratio is used, which is defined as the stopping power of the molecule divided by the sum of stopping powers of its atomic constituents.

The origin of these differences is due to the so-called *vicinage effects* in the electronic excitations produced by neighboring projectiles, leading to interferences in the excitation of individual and collective modes induced in the target by the swift charges. These effects produce a significant change in the average energy loss, which may be observed because the stopping ratio becomes different from unity.

The vicinage effects depend on the molecular geometry and velocity, as well as on the properties of the stopping medium. In this paper we will study the energy loss of a H_3^+ molecule in an amorphous carbon target, by an extension of a previous calculation [5], and we will discuss the dependence of the stopping ratio on the orientation of the H_3^+ molecule relative to its direction of motion.

Since we are interested only in swift molecular beams ($v > v_F$), where v_F is the Fermi velocity of the target electrons, we will neglect the effects of elastic collisions with target atoms, which produce the so-called nuclear stopping power and nuclear scattering; therefore, in what follows we will assume that all the energy loss is due to electronic interactions and that projectiles are undeflected by nuclear collisions. Then, two different processes take place: (i) the Coulomb repulsion between the three protons that compose the molecule, and (ii) the electronic interaction between the ions of the molecule and the target electrons. We consider in a first approach that these two processes can be thought of as independent, due to their very different time scales ($\sim 10^{-15}$ - 10^{-14} s for the Coulomb explosion, and $\sim 10^{-17}$ - 10^{-16} s for the electronic interactions); in other words, the approach follows the scheme of the Born-Oppenheimer approximation to separate the electronic and nuclear motion [6]. Therefore, it is possible to perform separate evaluations of the relative positions of the protons in the molecule, changing due to the mutual Coulomb repulsion, on one side, and the instantaneous electronic stopping power, as a function of these relative positions, on the other.

As a result of the screened Coulomb repulsion, the relative positions of the three protons of the H_3^+ molecule change as they travel through the target. This effect will be taken into account by numerical calculations of the relative motion of the molecular fragments in the solid. The dielectric formalism will be used to calculate the instantaneous stopping power of the H_3^+ molecule. The total stopping power of the H_3^+ molecule after crossing the foil will be finally obtained

as an average over the dwell time of the stopping powers evaluated at the instantaneous relative positions of the protons, and using the Coulomb explosion results to perform this average.

This paper is organized as follows. The dynamics of the Coulomb explosion is detailed in Sect. II, whereas in Sect. III we introduce the dielectric formalism developed to evaluate the stopping power of a molecule. The comparison of our calculations with the experimental data is presented and discussed in Sect. IV, and, finally, Sect. V contains the conclusions of this work.

II Coulomb explosion of the molecule

When a fast H_3^+ molecule interacts with a solid, its binding electrons are usually stripped off in the first atomic layers. In subsequent collisions with target electrons the protons participate in capture and loss processes; as a result of these processes each individual proton may be represented by an effective charge Z_i^* [7], which for velocities $v > v_0$, where v_0 is the Bohr velocity, becomes close to unity.

Therefore, due to the repulsion between the protons, a complete description of the stopping power of H_3^+ molecules in carbon foils requires the inclusion of the Coulomb forces between the protons, once the molecule enters in the solid. We have analyzed two cases: pure Coulomb repulsion and screened interaction. The screened Coulomb potential produced at a distance r by a proton with effective charge Z^* may be approximated by [8]

$$V(r) = \frac{Z^*}{r} e^{-r/a} \tag{1}$$

where $a = v/\omega_{\rm pl}$ is the screening length, due to the valence electrons in the solid; in the case of large a, the pure Coulomb potential is recovered. For amorphous carbon we use the plasmon peak of higher energy ($\omega_{\rm pl}$ = 0.945 a.u.), which gives the main contribution to the energy loss function [9]. Note that (1) corresponds to a velocity dependent interaction, because a and Z^* both depend on v. The dependence with the velocity of the effective charge will be taken from the work of Yarlagadda et al. [7]. Atomic units are used through all this work.

The structure of the H_3^+ molecule is an equilateral triangle whose average side length in equilibrium is $r_0 \simeq 1.89$ a.u. [10–12]. Using the Verlet algorithm [13], we solved numerically the set of Newton equations for the three protons subject to their mutual Coulomb repulsion; the effect of these forces is to increase the distances between the protons in the H_3^+ triangle without changing its shape. In Fig. 1 we depict the evolution of the instantaneous interproton distance of the H_3^+ molecule, $r(t)$, as a function of the travel time. We show the results for two different velocities, v = 2 a.u. and v = 5 a.u., both for the screened (solid lines) and unscreened (dashed lines) cases. The screened curves are always under the corresponding unscreened ones, the differences between both cases being larger the lower is the velocity. It can be observed that after the molecule enters the target (with $r = r_0$ at t = 0) the value of r grows initially slowly, reaching thereafter an asymptotic linear behaviour, with a slope that increases with the velocity. The curves in

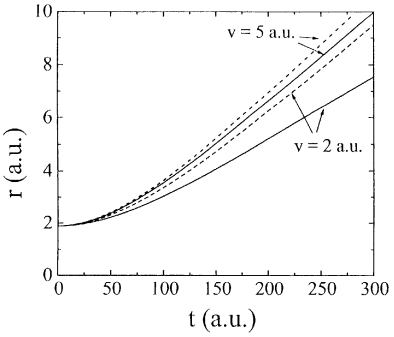

Fig. 1. Relation between interproton separation r and travelling time t, for two molecule velocities, v = 2 a.u. and v = 5 a.u. *Solid lines*: screened Coulomb potential, (1); *dashed lines*: unscreened Coulomb potential, (1) with $a = \infty$

Fig. 1 make it clear that the screening is more effective at lower velocities, due to the fact that the value of a increases with velocity. In this manner, the unscreened Coulomb case corresponds to the high velocity limit of the screened one. The stronger screening at low velocities can be understood by considering that, in this case, the valence electrons of carbon are fast enough to screen the charge of the protons.

III Electronic stopping power of a H_3^+ molecule

The electronic stopping power of a swift charge moving inside a solid is satisfactorily well described within the dielectric formalism, which was introduced by Fermi [14] and developed in further works [15–18]. In this formalism, the dynamic properties of an isotropic target are accounted for by its dielectric function $\epsilon(k,\omega)$, with k and ω representing, respectively, the momentum and energy transfers to the target electrons in an inelastic event.

The above formalism was applied [19] to study the electronic stopping power of a swift molecule or cluster. Within this scheme, the instantaneous stopping power of a H_3^+ molecule moving with velocity v through a target, with dielectric function $\epsilon(k,\omega)$, is given by [19]:

$$S_{H_3^+}(r_{ij},\theta_{ij}) = S_{\rm p}\left[\sum_{i=1}^{3} Z_i^{*2} + \sum_{i\neq j}^{3} Z_i^* Z_j^*\, I(r_{ij},\theta_{ij})\right] \tag{2}$$

where r_{ij} represents the relative position of protons i and j, and θ_{ij} gives the angle between the velocity $\mathbf{v}$ and the vector $\mathbf{r}_{ij}$ joining both protons. $S_{\rm p}$ is the proton stopping power, given by

$$S_{\rm p} = \frac{2}{\pi v^2}\int_0^\infty \frac{{\rm d}k}{k}\int_0^{kv} {\rm d}\omega\,\omega\,{\rm Im}\left[\frac{-1}{\epsilon(k,\omega)}\right] \tag{3}$$

Z_i^* is the effective charge of each proton in the molecule. We assume that the equilibrium charge state is reached for each constituent of the molecule, and that it is equal for atomic and molecular ions, i. e., $Z_i^* = Z^*$. The velocity dependent proton effective charge $Z_i^*(v)$ calculated by Yarlagadda et al. [7] will be used in our calculations.

For a set of values r and θ, the interference function $I(r,\theta)$ measures the vicinage effects that appear in the energy loss of correlated particles and it is given by [20]:

$$I(r,\theta) = \frac{2}{\pi v^2 S_p}\int_0^\infty \frac{dk}{k}\int_0^{kv} d\omega\,\omega\,\mathrm{Im}\left[\frac{-1}{\epsilon(k,\omega)}\right] \times \cos\left(\frac{z_0\omega}{v}\right) J_0(\rho_0\sqrt{k^2-\omega^2/v^2}) \quad (4)$$

In the above expression, $z_0 = r\cos\theta$ and $\rho_0 = r\sin\theta$ are the projections of the interproton distance parallel and perpendicular to the direction of motion, and $J_0(x)$ is the Bessel function of zero order.

The target properties are specified by its energy loss function, $\mathrm{Im}[-1/\epsilon(k,\omega)]$, whose momentum- and energy-dependence have been described in detail elsewhere [9, 21]; for the case of amorphous carbon the energy loss function was satisfactorily modeled by a sum of two Mermin-type functions that account for the contribution of the valence electrons at excitation energies less than the carbon K-edge, and for higher energies an extra Mermin-function was added to describe the contribution of the inner shell electrons to the electronic excitations. The Mermin dielectric function [22] is a generalization of the well-known Lindhard dielectric function for a free electron gas [23], by taking into account the finite plasmon lifetime (due to the decay into electron-hole excitations). For a carbon target, this damping mechanism turns out to be quite important in the context of stopping power phenomena [24, 25]. In this way we reproduce the two peaks in the energy loss function of amorphous carbon corresponding to the collective excitations of π and $\pi+\sigma$ valence electrons in carbon, which are found experimentally [26] at ~ 6 eV and ~ 26 eV.

For each velocity, we define the instantaneous stopping ratio R_3 of the H_3^+ molecule as the total stopping power of the H_3^+ molecule at velocity v divided by the sum of the stopping powers of three non-correlated protons with the same velocity v. For a given molecular orientation, the energy loss will depend on the interproton distance r, then we write

$$R_3(r) = \frac{S_{H_3^+}(r)}{3\,Z^{*2}\,S_p} \quad (5)$$

This quantity gives information about the vicinage effects produced by the correlated motion of the protons in the molecule. In particular, the value $R_3 = 1$ means that there are not interference effects, e.g., when the distances between the three protons in the molecule are large they slow down as three independent charges Z^*. The maximum value, $R_3 = 3$, occurs when the protons are so close together that they slow down like a single triply-charged particle, $3Z^*$.

According to (2) and (4), the stopping ratio for a given velocity depends on the interproton distance as well as on the molecular orientation with respect to the velocity. In Fig. 2 we show the H_3^+ molecule in two particular orientations: parallel and perpendicular to the direction of motion; the calculations for these orientations are easily made and the results will be quite different, as it will be seen later on.

Due to the Coulomb explosion the interproton distances grow with time, as discussed in Sect. II, and to a first approximation the equilateral triangular shape of the H_3^+ molecule is retained. Then it is convenient to evaluate the stopping ratio as a function of the instantaneous interproton distance r. For the case of the H_3^+ molecule oriented perpendicularly to its motion we have

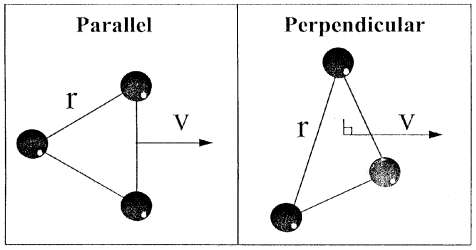

Fig. 2. Parallel and perpendicular orientation of the H_3^+ molecule relative to the incident beam direction

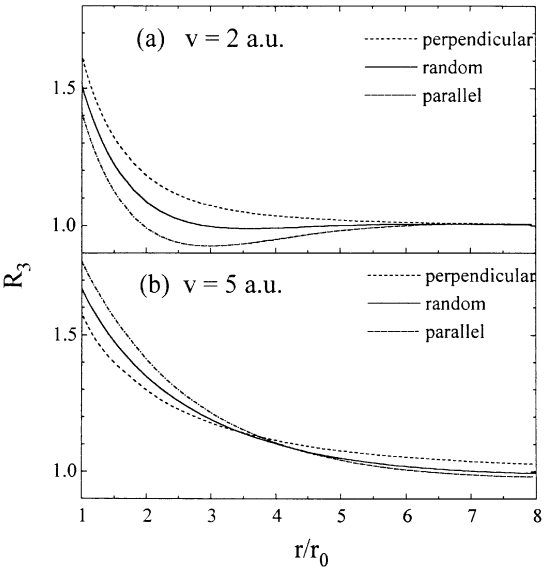

Fig. 3. Instantaneous stopping ratio, $R_3(r)$, as a function of the interproton separation, for perpendicular ($- - -$), parallel ($- \cdot - \cdot -$) and random (—) orientation of the H_3^+ molecule with respect to its velocity: **a** $v = 2$ a.u., and **b** $v = 5$ a.u.

$$R_3^\perp(r) = 1 + 2\,I(r,\theta=\pi/2) \quad (6)$$

while for the parallel orientation we get

$$R_3^\parallel(r) = 1 + \frac{2}{3}\left[2I(r,\theta=\pi/6) + I(r,\theta=\pi/2)\right] \quad (7)$$

Note that in this approximation the initial orientation, determined by the angle θ, does not change with time; this is so because we have assigned to $R_3^\perp$ and $R_3^\parallel$ a time-dependence only through $r(t)$. By symmetry and linearity considerations, $R_3^\parallel$ does not depend on whether the triangular structure of the molecule points towards or against the direction of motion.

The case of random orientation is closer to the experimental conditions [27], in which the initial orientations of the molecules are not controlled. In this case, the stopping ratio is given by

$$R_3^{ran}(r) = 1 + 2\,\langle I(r)\rangle \quad (8)$$

where $\langle I(r)\rangle$ denotes the angular average of $I(r,\theta)$.

In Fig. 3 we show the instantaneous stopping ratio of the H_3^+ molecule as a function of the interproton separation, for perpendicular, parallel and random orientations and for two different velocities. We notice that the vicinage effect produces a positive interference ($R_3 > 1$) for most cases, except for parallel orientation at low velocities, where a negative

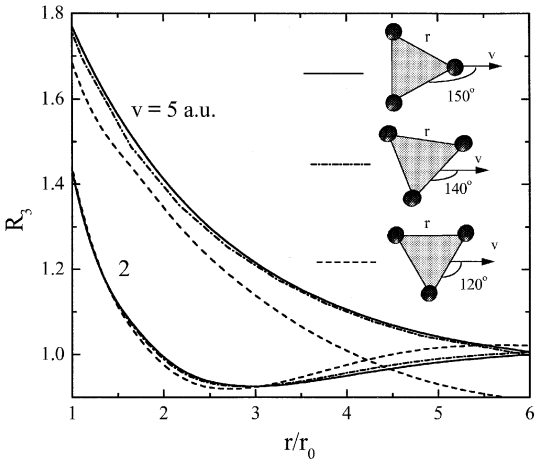

Fig. 4. Instantaneous stopping ratio, $R_3(r)$, as a function of the interproton separation, for three different parallel orientations. Results for two velocities, v = 2 a.u. and v = 5 a.u., are plotted

interference is found at intermediate values of r. At v = 5 a.u. the stopping ratio for the parallel case is larger than for the perpendicular one, while the opposite behaviour is found for v = 2 a.u. It can also be seen that for larger velocities the vicinage effects extend to larger interproton distances, and that $\lim_{r\to\infty}[R_3(r)] = 1$, which corresponds to the stopping of three uncorrelated protons. These results can be explained by a spatial analysis of dynamical screening effects and of the proton wake potential for different velocities [28]. To put it in a rather simple form, both the dynamical screening length, $a = v/\omega_{\rm pl}$, and the wake wavelength (to be discussed below), $\lambda \cong 2\pi v/\omega_{\rm pl}$, increase linearly with the velocity.

In order to know the influence of the different parallel orientations (not only the symmetric case we discussed previously) on the energy loss of the H_3^+ molecule, in Fig. 4 we show the stopping ratio calculated for three non-equivalent parallel orientations (with different internal-orientation angles) and for two velocities. It can be seen that for v = 2 a.u., the stopping ratio is practically the same for any parallel orientation and in a wide range of interproton separations, especially at the shorter ones. However, sizeable differences appear at higher velocities, as it can be appreciated when v = 5 a.u. For both velocities, the differences between the non-equivalent parallel orientations are larger the larger the interproton separation; these differences can be explained in terms of the wake potential (see next section). Further calculations for lower velocities show that all the curves for parallel orientation coincide very closely. These results are in accordance with previous calculations [20] showing that, in the low-velocity range, the stopping-ratio for parallel orientation of the molecular plane becomes independent of the internal orientation angle. This property is strictly valid in the low velocity limit, where it can be assumed that the energy loss function, $\mathrm{Im}[-1/\epsilon(k,\omega)]$, is linear in ω.

IV Results and discussion

The total stopping ratio $\overline{R_3}$ of the H_3^+ beam, after traversing a foil with thickness D, can be evaluated as the average of the instantaneous stopping ratio over the growing side

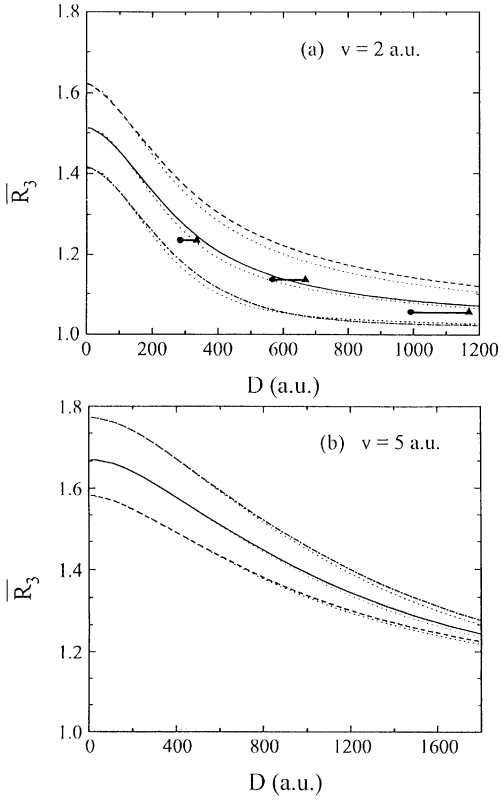

Fig. 5a,b. Total stopping ratio, $\overline{R_3}$, as a function of the carbon foil thickness, for the three molecule orientations: perpendicular (− − −), parallel (−·−·−) and random (—). The *thin dotted lines* correspond to the unscreened cases. **a** v = 2 a.u.; experimental data from Ray et al. [27] are plotted as *dots* (if we take ρ = 2 g/cm^3) and *triangles* (if we take ρ = 1.7 g/cm^3), joined by a horizontal bar. **b** v = 5 a.u

length that the H_3^+ molecule has during its travel inside the target. This r-average can be converted to a time-average taking into account the relation between r and t due to the Coulomb repulsion that is illustrated in Fig. 1. Then

$$\overline{R_3} = \frac{1}{\tau}\int_0^\tau \mathrm{d}t\, R_3(r(t)) \qquad (9)$$

where $\tau = D/v$ is the dwell time. For each molecular orientation, $R_3(r(t))$ in the previous equation should be replaced by the expressions given in (6)–(8), which correspond, respectively, to the perpendicular, parallel and random molecular orientations.

In Figs. 5a and 5b we present the H_3^+–stopping ratio $\overline{R_3}$, corresponding to these three molecular orientations, as a function of the thickness D of the carbon foil, and for two velocities, v = 2 a.u. and v = 5 a.u. The behaviours of $\overline{R_3^\perp}$, $\overline{R_3^\parallel}$ and $\overline{R_3^{\rm ran}}$ are quite similar, decreasing as the foil thickness increases. For both velocities, the stopping ratio for the random orientation lies between the perpendicular and the parallel cases; we find that $\overline{R_3^\perp} > \overline{R_3^\parallel}$ when v = 2 a.u. while the opposite is true when v = 5 a.u. To evaluate the effects of the screening in our calculations, we have accompanied each curve with a thin dotted line representing the results that one would obtain when using an unscreened Coulomb potential, i.e., $a = \infty$ in (1). We can observe that there are scarce differences with the screened cases, although

these are slightly larger at lower velocities. We can also see that the stopping ratio tends to unity for thicker foils, this tendency being faster for low-velocity molecules. We have incorporated to Fig. 5a the experimental results from Ray et al. [27]. The amorphous carbon density varies according to the preparation and measurement methods [29], and the commonly reported values are in the range 1.7 to 2 μg/cm^2. As the density of the amorphous carbon target was not indicated in these experiments [27], we have plotted in figure 5a their results as horizontal bars with their left extremes corresponding to a density 2μg/cm^2 and the right ones to 1.7 μg/cm^2. It can be observed a good agreement with the calculations corresponding to the randomly oriented molecules, which is the most likely experimental situation.

All these facts can be further understood by analyzing the wake potential $\phi_{\rm w}(\tilde{z},\rho)$ produced by a proton with velocity v. This wake is associated to charge oscillations induced in the target electrons by the moving projectile, and it can be written as [28]:

$$\phi_{\rm w}(\tilde{z},\rho) = \frac{2}{\pi v}\int_0^\infty \frac{{\rm d}k}{k}\int_0^{kv} {\rm d}\omega\, {\rm J}_0\left(\rho\sqrt{k^2-\omega^2/v^2}\right) \times\left\{\cos\left(\frac{\tilde{z}\omega}{v}\right)\,{\rm Re}\left[\frac{1}{\epsilon(k,\omega)}-1\right] -\sin\left(\frac{\tilde{z}\omega}{v}\right)\,{\rm Im}\left[\frac{1}{\epsilon(k,\omega)}-1\right]\right\}. \qquad (10)$$

This expression should be multiplied by Z^* to take into account the velocity dependence of the proton effective charge, but since Z^* acts only as a scaling factor, it will not affect the qualitative discussion that follows below. The cylindrical coordinates $\tilde{z}$ and ρ correspond to a reference frame that travels with the proton, and are defined by $\tilde{z} = z - vt$ and $\rho = (x^2 + y^2)^{1/2}$, relative to the position of the proton in a fixed reference frame, $(x_{\rm p}, y_{\rm p}, z_{\rm p}) = (0, 0, vt)$. To illustrate this point we show in Figs. 6a,ba and 6b the wake potential of a proton moving with velocities v = 2 a.u. and 5 a.u., respectively, in amorphous carbon. It can be seen that the wake potential has an oscillatory behaviour in the $\tilde{z}$ direction, with a wavelength $\lambda \sim 2\pi v/\omega_{\rm pl}$, and a nearly-exponential decrease in the transversal direction. The amplitude of this oscillatory wake is significantly damped because of the plasmon decay mechanism included in the Mermin dielectric function. Then, if the distance among the protons in the molecule is much larger than this wavelength, each proton will not feel the effects of its molecular partners; as a consequence, there will be no interference effects, i.e. $R_3 \cong 1$, resulting as if the three protons were moving in an uncorrelated way.

The wake potential obtained here may be compared with the results one would obtain using a simple Lindhard dielectric function. In the former case, a stronger damping of the wake potential is predicted, giving rise to a faster cancellation of the vicinage effects with increasing interproton distances. A detailed comparison of the wake potentials calculated using different dielectric models for various materials will be reported elsewhere [30].

The orientational behaviour of the stopping power can also be explained by the study of the wake potential. If the plane of the molecule is oriented parallel to its motion, there is at least one proton behind another, in such a way that under particular conditions the wake force acting on the

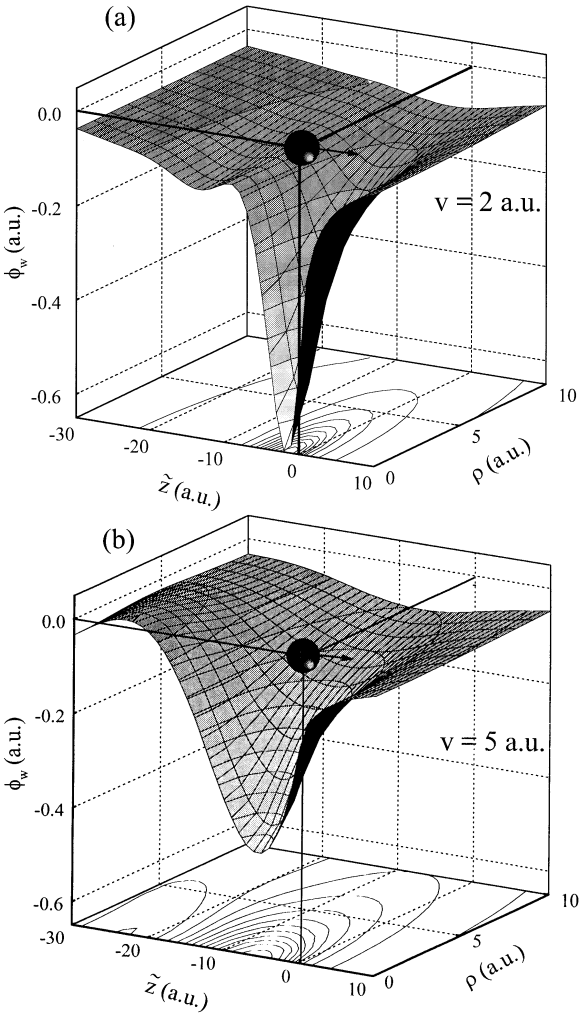

Fig. 6a,b. Wake potential of a proton moving in amorphous carbon, in cylindrical coordinates relative to the instantaneous position of the proton. **a** v = 2 a.u. **b** v = 5 a.u.

trailing one could be an accelerating force (corresponding to a negative slope of the wake potential). If this accelerating force becomes larger than the retarding interference forces acting on the rest of the particles, then a negative interference effect may be obtained, and then $R_3(r) < 1$, as found in Fig. 3a. In the case of perpendicular orientation this effect does not occur and the interference forces acting on the protons are always retarding ones (as well as the self-induced forces in all the cases). In the case of parallel orientation it can be seen that, due to the velocity dependence of the wake wavelength, negative interferences appear at larger interproton distances, as v increases (see Fig. 4); also, R_3 tends more slowly to unity the greater is v, because in this case wake effects last for larger distances (see Figs. 6). The shape of the wake is also responsible that at high velocities a maximum in the negative interference takes place when a trailing proton is aligned with the leading one (dashed curve in Fig. 4, when v = 5 a.u.), therefore a departure from this alignment strongly reduces these effects.

Finally, in Fig. 7 we show the stopping ratio suitable for comparison with experiments, i.e., $\overline{R_3^{\rm ran}}$, as a function of the beam energy and for three foil thicknesses: 3, 6 and 10.5

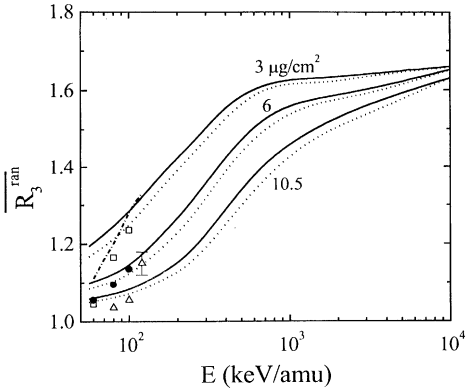

Fig. 7. $\overline{R_3^{ran}}$ as a function of the energy of the H_3^+ beam, for three target thicknesses. The *solid lines* represent our results for a carbon density of 2 g/cm^3, while the *dotted lines* correspond to a density of 1.7 g/cm^3. The experimental data were taken from [27]: 3 μg/cm^2, *empty squares*; 6 μg/cm^2, *filled circles*, and 10.5 μg/cm^2, *empty triangles*. The theoretical estimates by Ray et al. [27] for 3 μg/cm^2 are represented by a *dashed line*

μg/cm^2. This calculation was obtained taking into account the contribution to the energy loss processes of the valence and the core electrons of carbon; the effect of the latter is to reduce the value of $\overline{R_3^{ran}}$ at energies larger than ~ 1 MeV/amu, a result that was already pointed out by Kaneko [31]. Our results are compared with the experimental data obtained by Ray et al. [27] and the theoretical calculations for 3 μg/cm^2 reported by the same authors. We made our calculations for the two values of the amorphous carbon density previously quoted: 1.7 g/cm^3 and 2 g/cm^3. The results corresponding to the former case are plotted as dotted lines, while those for the latter one appear as solid lines in Fig. 7; the experimental data are shown as different symbols for each one of the three target thicknesses, and the calculation by Ray et al. is depicted as a dashed line. The comparison with the experimental data and the other theoretical estimate may be considered satisfactory, showing the same trends for each target thickness, giving stopping ratios larger than unity, decreasing with the target thickness and growing with the projectile energy. The shape of the curve $\overline{R_3^{ran}}$ *vs.* E flattens for the thinner targets as the energy increases.

The lack of experimental data at higher energies does not allow us to make a more complete test of the theoretical predictions. The recent measurements by Susuki et al. [32] have brought interesting data on the energy loss of transmitted H_3^+ molecules –i.e., those few molecular ions which survive the passage through the foil, and hence do not experience the Coulomb explosion effects studied here. For this reason, the values reported by Susuki et al. cannot be compared with the present calculations; however, their result show that at ~ 10 MeV/amu the energy loss of H_3^+ is nearly independent of the target thickness, and the same trend can be seen in the high energy region of Fig. 7. The physical interpretation of this lies in the short dwell time at such high energies, for which the internuclear distances almost do not change while the molecule travels inside the target, within the range of thicknesses considered here.

V Conclusions

We have applied a dielectric formalism [19] to calculate the energy loss of H_3^+ molecular beams in amorphous carbon foils, using an accurate description of the dielectric properties of the target [9], and including in our treatment the dynamics of the molecular explosion, due to Coulomb repulsion among the protons. We have performed a detailed study of the dependence of the stopping ratio with the energy and orientation of the molecule, for different target thicknesses. The orientational effects show some qualitative changes with velocity. The stopping ratio of H_3^+ molecules at high velocities is larger for parallel than for perpendicular orientation, while the opposite occurs at low or intermediate velocities. Besides, the interference effects in the energy loss may be negative at some interproton distances, especially for intermediate velocities and parallel orientation. A detailed analysis of the orientational effects can be made by considering the spatial variation of the induced wake potential. This was done here by using a realistic representation of the dielectric function of amorphous carbon in terms of Mermin-type response functions.

The experimentally measurable stopping ratio was calculated as the average of the instantaneous stopping ratio, while the interproton distances grow as the molecule travels inside the target. Further calculations, including the distortion of the molecular structure due to nuclear scattering and to unequal wake forces on each proton, besides to Coulomb explosion, deserve a special treatment and will be published in a forthcoming paper. However, the results obtained with the present model for randomly oriented molecular beams show a good agreement with the available experimental results.

This work was supported in part by the Spanish Dirección General de Investigación Científica y Técnica (projects PB93-1125 and PB95-0689). CDD thanks the Instituto de Cooperación Iberoamericana for a doctoral fellowship. NRA wishes to thank the Conselleria d'Educació i Ciència de la Generalitat Valenciana for a visiting professor fellowship to the Universitat d'Alacant under the program PROPIO.

References

1. Proceedings of the Conference on Polyatomic Ion Impact on Solids and Related Phenomena, Saint-Malo (1993) [Nucl. Instrum. Meth. B **88**, 1 (1994)]
2. Interaction of Charged Particles with Solids and Surfaces, NATO ASI Series Vol. B 271, edited by A. Gras-Martí, H. M. Urbassek, N. R. Arista and F. Flores (Plenum, New York, 1990)
3. Proceedings of the International School of Plasma "Physics on Inertial Confinement Fusion", edited by A. Caruso and E. Sindoni (Compositori, Bologna, 1988)
4. W. Brandt, A. Ratkowski and R. H. Ritchie, Phys. Rev. Lett. **33**, 1325 (1974)
5. C. D. Denton, F. J. Pérez-Pérez, I. Abril, R. Garcia-Molina and N. R. Arista, Europhys. Lett. **35**, 499 (1996)
6. N. F. Mott and H. S. W. Massey, The Theory of Atomic Collisions. Oxford: Oxford University Press 1950
7. B. S. Yarlagadda, J. E. Robinson and W. Brandt, Phys. Rev. B **17**, 3473 (1978)
8. W. Brandt, p.261 in Atomic Collisions in Solids, Vol. 1, edited by S. Datz, B. R. Appleton and C. D. Moak (Plenum, New York, 1975)
9. I. Abril, R. Garcia-Molina and N. R. Arista, Nucl. Instrum. Meth. B **90**, 72 (1994)

10. M. J. Gaillard, D. S. Gemmell, G. Goldring, I. Levine, W. J. Pietsch, J.-C. Poizat, A. J. Ratkowski, J. Remillieux, Z. Vager and B. J. Zabransky, Phys. Rev. A **17**, 1797 (1978)
11. G. D. Carney, Molec. Phys. **39**, 923 (1980)
12. D. S. Gemmell, Nucl. Instrum. Meth. **191**, 425 (1981)
13. M. P. Allen and D. J. Tildesley, Computer Simulation of Liquids. Oxford: Oxford Science Publications 1987
14. E. Fermi, Z. Physik **29**, 315 (1924)
15. E. Fermi, Phys. Rev. **57**, 485 (1940)
16. J. Hubbard, Proc. Phys. Soc. (London) A **68**, 976 (1955)
17. J. Neufeld and R. H. Ritchie, Phys. Rev. **98**, 1632 (1955)
18. P. Nozières and D. Pines, Phys. Rev. **113**, 1254 (1959)
19. N. R. Arista, Phys. Rev. B **18**, 1 (1978)
20. N. R. Arista and A. Gras-Martí, J. Phys. Cond. Matter **3**, 7931 (1991)
21. D. J. Planes, R. Garcia-Molina, I. Abril and N. R. Arista, J. Electr. Spectrosc. Relat. Phenom. **82**, 23 (1996)
22. N. D. Mermin, Phys. Rev. B **1**, 2362 (1970)
23. J. Lindhard, Mat. Fys. Medd. Dan. Vid. Selsk. **28**, No. 8 (1954)
24. M. W. Williams, E. T. Arakawa, J. Appl. Phys. **43**, 3460 (1972)
25. J. C. Ashley and P. M. Echenique, Phys. Rev. B **31**, 4655 (1985)
26. J. Cazaux and P. Gramari, J. de Phys. **38**, L133 (1977)
27. E. Ray, R. Kirsch, H. H. Mikkelsen, J. C. Poizat and J. Remillieux, Nucl. Instrum. Meth. B **69**, 133 (1992)
28. P. M. Echenique, R. H. Ritchie and W. Brandt, Phys. Rev. B **20**, 2567 (1979)
29. J. O. Stoner, Nucl. Instrum. Meth. A **303**, 94 (1991)
30. I. Abril, R. Garcia-Molina, C. D. Denton F. J. Pérez-Pérez, and N. R. Arista (to be published)
31. T. Kaneko, Phys. Rev. A **51**, 535 (1995)
32. Y. Susuki, M. Fritz, K. Kimura, M. Mannami, N. Sakamoto, H. Ogawa, I. Katayama, T. Noro and H. Ikegami, Phys. Rev. A **51**, 3868 (1995)